Commun. Comput. Phys.
doi: 10.4208/cicp.241110.280111a

Vol. **10**, No. 4, pp. 899-911
October 2011

Gyrokinetic Simulation of Magnetic Compressional Modes in General Geometry

Peter Porazik[1] and Zhihong Lin[1,*]

Department of Physics and Astronomy, University of California, Irvine, CA 92697, USA.

Received 24 November 2010; Accepted (in revised version) 28 January 2011

Communicated by Xueqiao Xu

Available online 13 June 2011

Abstract. A method for gyrokinetic simulation of low frequency (lower than the cyclotron frequency) magnetic compressional modes in general geometry is presented. The gyrokinetic-Maxwell system of equations is expressed fully in terms of the compressional component of the magnetic perturbation, $\delta B_{\parallel}$, with finite Larmor radius effects. This introduces a "gyro-surface" averaging of $\delta B_{\parallel}$ in the gyrocenter equations of motion, and similarly in the perpendicular Ampere's law, which takes the form of the perpendicular force balance equation. The resulting system can be numerically implemented by representing the gyro-surface averaging by a discrete sum in the configuration space. For the typical wavelength of interest (on the order of the gyroradius), the gyro-surface averaging can be reduced to averaging along an effective gyro-orbit. The phase space integration in the force balance equation can be approximated by summing over carefully chosen samples in the magnetic moment coordinate, allowing for an efficient numerical implementation.

PACS: 02.60.-x, 02.70.-c, 52.65.Tt

Key words: Finite Larmor radius effects, gyrokinetic simulation, compressional modes, gyro-surface average.

1 Introduction

The low frequency compressional magnetic perturbations, $\delta B_{\parallel}$, are commonly neglected in gyrokinetic simulations [17, 20, 22], which assume a low β plasma (β is the ratio of kinetic pressure to magnetic pressure). As β increases the role of $\delta B_{\parallel}$ becomes more important due to plasma diamagnetism, and may no longer be neglected. The finite β introduces new modes, such as the magnetic trapped particle mode [26], the drift mirror mode [12], or the drift compressional mode [13], in which $\delta B_{\parallel}$ is a dominant field

*Corresponding author. *Email addresses:* pporazik@uci.edu (P. Porazik), zhihongl@uci.edu (Z. Lin)

perturbation. Even in low β plasmas the compressional component of the magnetic perturbation may have to be considered [15].

A numerical difficulty in gyrokinetic simulation of compressional modes is the calculation of finite Larmor radius effects in general geometry. Various numerical techniques have been used in the past to take into account the finite Larmor radius in the gyrokinetic simulations containing nonzero compressional component of the perturbed magnetic field ($\delta B_\parallel$). One of the key features that distinguishes these techniques is how they implement gyro-orbit averaging. In case of low frequency compressional modes (mode frequency smaller than ion cyclotron frequency), the gyro-orbit averaged quantity has been cast into the form of $\langle \delta \mathbf{A}_\perp \cdot \mathbf{v}_\perp \rangle$, where $\delta \mathbf{A}_\perp$ is the component of the vector potential perpendicular to the equilibrium magnetic field ($\delta B_\parallel = \hat{\mathbf{b}} \cdot \nabla \times \delta \mathbf{A}_\perp$), $\mathbf{v}_\perp$ is the perpendicular component of the particle velocity, $\hat{\mathbf{b}}$ is the unit vector along the equilibrium magnetic field, and $\langle \cdots \rangle$ stands for the gyro-orbit average. In simulations implementing a pseudo-spectral method in a simple geometry, the gyro-orbit averages may be performed analytically for each spectral component [16]. Another approach has been to perform the gyro-orbit averages explicitly in configurations space, using the method described in [17] and [21] to solve the gyrokinetic Vlasov-Poisson system; and extended in [18] to an electromagnetic case. The method is to average the quantity $\delta \mathbf{A}_\perp \cdot \mathbf{v}_\perp$ directly in configuration space, over a finite number of samples along the gyro-orbit. Variations of this technique were used in hybrid simulations of energetic particle effects on low frequency MHD modes in [2], and gyrokinetic simulations of the mirror mode in [25].

In the gyrokinetic theory [1,3–7,10,19,24,27], the fundamental operation of gyro-orbit averaging reduces the number of dynamical variables from six, in the particle phase space ($\mathbf{x}$,$\mathbf{v}$), to five in the gyrocenter phase space ($\mathbf{X}$,$v_\parallel$,μ). This, in turn, results in the decrease of the number of independent field quantities appearing in the Maxwell's equations. Thus, the perpendicular Ampere's law has now only one degree of freedom. Adopting the convention of [8], the independent quantities are the electrostatic potential, ϕ; the parallel component of the vector potential, $\delta A_\parallel$; and the compressional component of the magnetic perturbation, $\delta B_\parallel$. It is then undesirable to use $\delta \mathbf{A}_\perp$ rather than $\delta B_\parallel$ in gyrokinetic simulation models, from either a numerical or a physical standpoint, since $\delta B_\parallel$ is a scalar and a more physical and fundamental field quantity than $\delta \mathbf{A}_\perp$. In the current work, a gyrokinetic system for low frequency compressional modes in general geometry is expressed fully in terms of the compressional component of the magnetic perturbation, $\delta B_\parallel$. This introduces a "gyro-surface" average of $\delta B_\parallel$ in the gyrocenter equations of motion, and similarly in the perpendicular Ampere's law, which takes the form of the low frequency perpendicular force balance equation. The resulting system may be numerically approximated by representing the gyro-surface averaging by a discrete sum in the configuration space. For the typical wavelength of interest (on the order of the gyroradius), the gyro-surface averaging may be reduced to averaging along an effective gyro-orbit, for an efficient numerical implementation. The phase space integration which appears in the low frequency force balance equation, may be approximated by carefully

choosing samples in the magnetic moment coordinate, and their corresponding weights.

The next section outlines the gyrokinetic simulation model for the low frequency compressional modes. In Section 3.1 the gyrocenter equations of motion are expressed in terms of $\delta B_{\parallel}$, and Section 3.2 discusses a method of numerical implementation. The perpendicular Ampere's law is discussed in Section 4.1, and a numerical implementation is presented in Section 4.2. The conclusions are given in Section 5.

2 Simulation model for compressional modes

The gyrokinetic system of equations, for the simplest description of the compressional modes, consists of the ion gyrokinetic equation [4],

$$\left(\partial_t+\dot{\mathbf{X}}\cdot\nabla+\dot{v}_{\parallel}\partial_{v_{\parallel}}\right)F=0, \tag{2.1}$$

the ion gyrocenter equations of motion,

$$\dot{\mathbf{X}}=v_{\parallel}\hat{\mathbf{b}}+\frac{\hat{\mathbf{b}}}{m\Omega_i}\times\left(\mu B_0\nabla\ln B_0+mv_{\parallel}^2\hat{\mathbf{b}}\cdot\nabla\hat{\mathbf{b}}\right)-\frac{c}{B_0}\hat{\mathbf{b}}\times\nabla\left\langle\delta\mathbf{A}_{\perp}\cdot\frac{\mathbf{v}_{\perp}}{c}\right\rangle, \tag{2.2a}$$

$$\dot{v}_{\parallel}=-\frac{1}{m}\hat{\mathbf{b}}\cdot\nabla\left(\mu B_0-e\left\langle\delta\mathbf{A}_{\perp}\cdot\frac{\mathbf{v}_{\perp}}{c}\right\rangle\right)+\frac{cv_{\parallel}}{B_0}\hat{\mathbf{b}}\times\left(\hat{\mathbf{b}}\cdot\nabla\hat{\mathbf{b}}\right)\cdot\nabla\left\langle\frac{\mathbf{v}_{\perp}}{c}\cdot\delta\mathbf{A}_{\perp}\right\rangle, \tag{2.2b}$$

and the perpendicular Ampere's law,

$$\nabla_{\perp}\delta B_{\parallel}\times\hat{\mathbf{b}}=4\pi\frac{e}{c}\int d^3v\mathbf{v}_{\perp}\delta f; \tag{2.3}$$

where $\delta f=f-f_0$ is the perturbed particle distribution function. The definitions of various symbols in (2.1)-(2.3) are, $(\mathbf{X},v_{\parallel},\mu)$ is a set of gyrocenter variables standing for gyrocenter position, parallel velocity, and magnetic moment, respectively [3]; $\Omega_i=eB_0/mc$ is the cyclotron frequency; $\hat{\mathbf{b}}=\hat{\mathbf{e}}_1\times\hat{\mathbf{e}}_2$ is the unit vector pointing along the equilibrium magnetic field at the particle position; $\delta F=F-F_0$ is the perturbed gyrocenter distribution function; F_0 is assumed to be the Maxwellian distribution,

$$F_0=n_0\sqrt{\frac{m^3}{(2\pi T_i)^3}}\exp\left[-T_i^{-1}\left(\frac{mv_{\parallel}^2}{2}+\mu B_0\right)\right],$$

$\delta B_{\parallel}$ is the magnetic perturbation parallel to the equilibrium magnetic field; $\delta\mathbf{A}_{\perp}$ is the perturbed vector potential perpendicular to the equilibrium magnetic field; and $\langle\cdots\rangle$ stands for the gyro-orbit average, performed by the operation $\frac{1}{2\pi}\oint\cdots d\xi$, where ξ represents the gyro-angle. The assumption that electrons are cold and the frequency of interest is much lower than shear Alfvén frequency, allows neglecting $\delta\phi$, $\delta A_{\parallel}$ and electron contribution in the Ampere's law [9], focusing purely on compressional modes. The formulation and implementation for gyrokinetic simulations of $\delta\phi$ and $\delta A_{\parallel}$ have been extensively published, for example [14] and references therein. Details about the derivation of a gyrokinetic system of equations may be found, for example, in the review given in [5].

3 Equation of motion in terms of $\delta B_{\parallel}$

In Section 3.1 the gyrocenter equations of motion are expressed in terms of $\delta B_{\parallel}$, and in Section 3.2 the numerical implementation of gyroaveraging is discussed.

3.1 Gyro-surface averaging of $\delta B_{\parallel}$

The field quantity $\delta\mathbf{A}_{\perp}$ appears in the equations of motion, Eqs. (2.2a) and (2.2b), in the combination $\langle\delta\mathbf{A}_{\perp}\cdot\mathbf{v}_{\perp}\rangle$. Using the relationship of the differential displacement vector, $d\mathbf{l}$, to the perpendicular velocity, $\mathbf{v}_{\perp}$, and to the Larmor radius, $\boldsymbol{\rho}$, given by $d\mathbf{l}=(\boldsymbol{\rho}\times\hat{\mathbf{b}})d\xi$, as shown in Fig. 1; applying the Stoke's theorem; and using all vector components of $\nabla\times\delta\mathbf{A}=\delta\mathbf{B}$, $\langle\delta\mathbf{A}_{\perp}\cdot\mathbf{v}_{\perp}\rangle$ may be expressed in terms of $\delta\mathbf{B}$ as

$$\langle\delta\mathbf{A}\cdot\mathbf{v}_{\perp}\rangle=\frac{\Omega_i}{2\pi}\int_S d\mathbf{S}\cdot\delta\mathbf{B}. \tag{3.1}$$

$\langle\delta\mathbf{A}\cdot\mathbf{v}_{\perp}\rangle$ is thus proportional to the change in the magnetic flux through the gyro-orbit–a quantity reminiscent of the induced electromotive force. Since $d\mathbf{S}$ is the differential of the area enclosed by the gyro-orbit whose direction is given by the right-hand rule in relation to the sense of the gyration of the charged particle, $d\mathbf{S}=-\hat{\mathbf{b}}dS$; and since

$$\int\cdots dS=\int_0^{2\pi}\int_0^{\rho}\cdots rdrd\xi,$$

then also

$$\langle\delta\mathbf{A}\cdot\mathbf{v}_{\perp}\rangle=-\Omega_i\Big\langle\int_0^{\rho}\delta B_{\parallel}rdr\Big\rangle=-\frac{c}{e}\mu\langle\langle\delta B_{\parallel}\rangle\rangle, \tag{3.2}$$

where

$$\langle\langle\cdots\rangle\rangle\equiv\frac{1}{\pi\rho^2}\int_0^{2\pi}\int_0^{\rho}\cdots rdrd\xi$$

is the "gyro-surface" average, with r being the gyroradius variable. Therefore, the gyro-orbit averaging of $\delta\mathbf{A}_{\perp}\cdot\mathbf{v}_{\perp}$ is equivalent to gyro-surface averaging of $\delta B_{\parallel}$.

A numerical representation of the gyro-surface averaging may be verified against an analytic expression in the Fourier space by letting

$$\delta B_{\parallel}(\mathbf{x},t)=e^{i\mathbf{r}\cdot\mathbf{k}_{\perp}}\delta B_{\parallel}(\mathbf{X},t),$$

where $\mathbf{r}$ is the position vector pointing from the gyrocenter position ($\mathbf{X}$) to the particle position. The integral appearing in Eq. (3.2) may then be performed, yielding

$$\langle\langle\delta B_{\parallel}\rangle\rangle=\delta B_{\parallel}(\mathbf{X},t)\frac{2}{k_{\perp}\rho}J_1(k_{\perp}\rho), \tag{3.3}$$

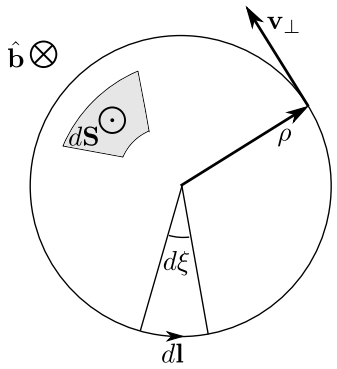

Figure 1: Relationship of various vectors involved in expressing $\langle \delta \mathbf{A}_\perp \cdot \mathbf{v}_\perp \rangle$ in terms of $\delta B_\parallel$. The displacement vector along the gyro-orbit is related to the perpendicular velocity of the gyrating charge (in this case, proton), $\mathbf{v}_\perp$, and its Larmor radius, $\boldsymbol{\rho}$, by $d\mathbf{l} = (\boldsymbol{\rho} \times \hat{\mathbf{b}}) d\xi$.

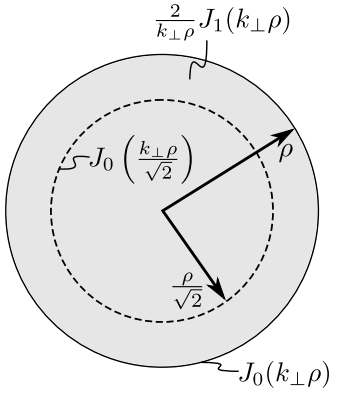

Figure 2: The average over the surface (shaded area) enclosed by the gyro-orbit (solid circle), which appears in Eq. (3.2), may be approximated by averaging over the effective gyro-orbit with the radius of $\rho/\sqrt{2}$ (dashed circle).

since $\mathbf{r} \cdot \mathbf{k}_\perp = r k_\perp \cos\xi$, because the origin of ξ is arbitrary; and

$$\left\langle \left\langle e^{i r k_\perp \cos\xi} \right\rangle \right\rangle = \frac{2}{k_\perp \rho} J_1(k_\perp \rho).$$

Here, J_1 is the first order Bessel function of the first kind.

In the dimensionless form, the problem thus reduces to numerically approximating the double integral on the left-hand side of

$$\frac{1}{\pi a^2} \int_0^{2\pi} \int_0^a e^{iu\cos\xi} u \, du \, d\xi = \frac{2}{a} J_1(a), \tag{3.4}$$

to reproduce the result on the right-hand side as closely as possible, where $a = k_\perp \rho$, and $u = k_\perp r$.

3.2 Numerical implementation

Numerical implementation involves spatial discretization of the integral over the surface enclosed by the gyro-orbit. Since it is straightforward to implement a gyro-orbit average to recover the 0^{th} order Bessel function J_0, the simplest approximation may be obtained using the Bessel function identity

$$\frac{2}{a}J_1(a)=J_0(a)-J_2(a), \tag{3.5}$$

which suggests that, since for long wavelength perturbations $J_0 \gg J_2$, in this limit the integral may be approximated by keeping only J_0 in Eq. (3.5), i.e., simple averaging over the gyro-orbit. However, the accuracy can be significantly improved by averaging over an "effective" gyro-orbit. The optimum effective gyro-orbit may be found by expanding both sides of

$$\frac{2}{a}J_1(a)\approx J_0(b), \tag{3.6}$$

in the limit $a\to 0$, and matching the 2^{nd} order terms. The result is $b=a/\sqrt{2}$. Consequently, in the limit $a\to 0$,

$$\frac{2}{a}J_1(a)\approx J_0\Big(\frac{a}{\sqrt{2}}\Big)+\mathcal{O}(a^4). \tag{3.7}$$

The numerical approximation of the double integral in Eq. (3.4) may then be explicitly represented by the discrete sum

$$\frac{1}{\pi a^2}\int_0^{2\pi}\int_0^a e^{iu\cos\xi}ududd\xi\approx\frac{1}{M}\sum_{m=1}^{M}\exp\Big[i\frac{a}{\sqrt{2}}\cos\Big(\frac{2\pi m}{M}\Big)\Big], \tag{3.8}$$

where M corresponds to the number of grid points in the gyroangle, ξ. An approximation for $M=4$, i.e., the widely used 4-point gyro-averaging [17], is shown in Fig. 3, together with the relative error. It can be seen that for the range of $a=k_\perp\rho\lesssim 3$ the approximation is close to being exact, even for this small value of M. Thus, it is sufficient to use 4 points around the gyrocenter, at an effective gyroradius of $\rho/\sqrt{2}$, to numerically approximate the average of $\delta B_\parallel$ over the surface enclosed by the gyro-orbit appearing in Eq. (3.2).

4 Perpendicular Ampere's law in terms of $\delta B_\parallel$

Due to the low frequency assumption, the fast magnetosonic waves are removed from the gyrokinetic theory, and the perpendicular Ampere's law can be written as a low frequency perpendicular force balance equation, which is entirely expressible in terms of $\delta B_\parallel$. The objective of this section is to derive an expression for the low frequency perpendicular force balance equation, in terms of $\delta B_\parallel$, and develop a numerical method for its evaluation in real space. This is done in Sections 4.1 and 4.2, respectively.

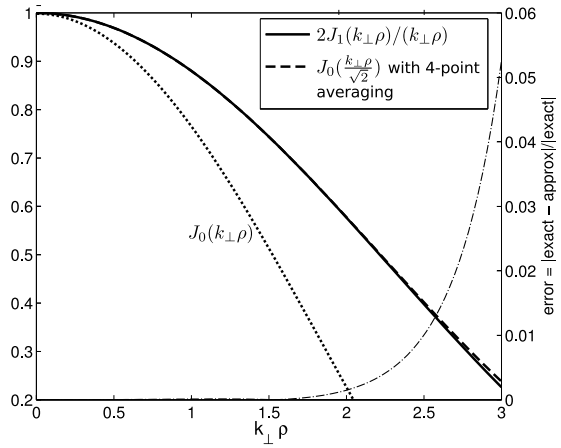

Figure 3: Comparison of the approximation of the double integral in (3.3), using (3.8) and $M=4$ (dashed line), to the exact result $2J_1(k_\perp\rho)/(k_\perp\rho)$ (solid line). The interrupted line is the relative error. The dotted black line corresponds to the approximation using $J_0(k_\perp\rho)$.

4.1 Analytic expression

Using the relation between particle and gyrocenter perturbed distribution for an isotropic Maxwellian equilibrium F_0,

$$\delta f=\delta F-\frac{e}{T_i}F_0\Big\langle\delta\mathbf{A}\cdot\frac{\mathbf{v}_\perp}{c}\Big\rangle,$$

see [4,5], the perpendicular Ampere's law (2.3) may be written as,

$$\nabla_\perp\delta B_\parallel\times\hat{\mathbf{b}}=4\pi\frac{e}{c}\int d^3v\mathbf{v}_\perp\Big(\delta F-\frac{e}{T_i}F_0\Big\langle\delta\mathbf{A}\cdot\frac{\mathbf{v}_\perp}{c}\Big\rangle\Big). \tag{4.1}$$

Using

$$d^3v=\frac{B_0}{m}d\mu dv_\parallel d\xi,\quad \mathbf{v}_\perp=\Omega_i\boldsymbol{\rho}\times\hat{\mathbf{b}},\quad d\mathbf{l}=-\big(\boldsymbol{\rho}\times\hat{\mathbf{b}}\big)d\xi,$$

as shown in Fig. 4, the integral appearing on the right-hand side of Eq. (4.1) becomes,

$$\int\frac{B_0}{m}d\mu dv_\parallel\int_0^{2\pi}\mathbf{v}_\perp\Big(\delta F-\frac{e}{T_i}F_0\Big\langle\delta\mathbf{A}\cdot\frac{\mathbf{v}_\perp}{c}\Big\rangle\Big)d\xi=-\int\frac{B_0}{m}d\mu dv_\parallel\oint\Omega_i\Big(\delta F-\frac{e}{T_i}F_0\Big\langle\delta\mathbf{A}\cdot\frac{\mathbf{v}_\perp}{c}\Big\rangle\Big)d\mathbf{l}. \tag{4.2}$$

Unlike in Section 3, the direction of $d\mathbf{l}$ is opposite to $\mathbf{v}_\perp$, since $d\mathbf{l}$ in Eq. (4.2) is not along the gyro-orbit, because the $d\xi$ integration in the present case comes from the summation over the contributions from gyrocenters lying $\boldsymbol{\rho}$ away from the particle, and not gyro-orbit averaging. Using

$$\oint gd\mathbf{l}=\int_S d\mathbf{S}\times\nabla g\quad\text{and}\quad d\mathbf{S}=-\hat{\mathbf{b}}rdrd\xi,$$

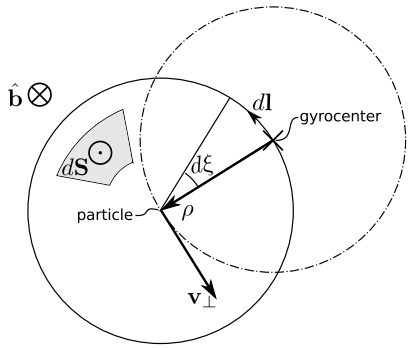

Figure 4: Vectors involved in expressing the perpendicular Ampere's law in terms of $\delta B_\parallel$.

the integral becomes,

$$\begin{aligned}&-\int\frac{B_0}{m}d\mu dv_\parallel\int_S d\mathbf{S}\times\nabla\Big\{\Omega_i\Big(\delta F-\frac{e}{T_i}F_0\Big\langle\delta\mathbf{A}\cdot\frac{\mathbf{v}_\perp}{c}\Big\rangle\Big)\Big\}\\&=\int\frac{B_0}{m}d\mu dv_\parallel\int_0^{2\pi}\int_0^\rho rdrd\xi\hat{\mathbf{b}}\times\nabla\Big\{\Omega_i\Big(\delta F-\frac{e}{T_i}F_0\Big\langle\delta\mathbf{A}\cdot\frac{\mathbf{v}_\perp}{c}\Big\rangle\Big)\Big\}.\end{aligned}\tag{4.3}$$

Finally, using Eq. (3.2) to remove $\delta\mathbf{A}$, it is found that

$$\begin{aligned}&\int\frac{B_0}{m}d\mu dv_\parallel\int_0^{2\pi}\int_0^\rho rdrd\xi\hat{\mathbf{b}}\times\nabla\Big\{\Omega_i\Big(\delta F-\frac{e}{T_i}F_0\Big\langle\delta\mathbf{A}\cdot\frac{\mathbf{v}_\perp}{c}\Big\rangle\Big)\Big\}\\&=2\pi\int\frac{B_0}{m}d\mu dv_\parallel\Big\langle\int_0^\rho\hat{\mathbf{b}}\times\nabla\Big\{\Omega_i\delta F+\frac{e}{cT_i}F_0\Omega_i^2\Big\langle\int_0^\rho\delta B_\parallel r'dr'\Big\rangle\Big\}rdr\Big\rangle.\end{aligned}\tag{4.4}$$

Using $2\pi/Lk_\perp\ll1$, the $\hat{\mathbf{b}}\times\nabla$ operator can be taken out of the integral and removed from the Ampere's law (4.1), which then becomes

$$\delta B_\parallel+\frac{8\pi^2\Omega_i^2}{\rho_i^2B_0}\int d\mu dv_\parallel F_0\Big\langle\int_0^\rho\Big\langle\int_0^\rho\delta B_\parallel r'dr'\Big\rangle rdr\Big\rangle=-8\pi^2\Omega_i^2\int d\mu dv_\parallel\Big\langle\int_0^\rho\delta Frdr\Big\rangle,\tag{4.5}$$

where

$$\rho_i\equiv\frac{v_{thi}}{\Omega_i},\quad v_{thi}\equiv\frac{T_i}{m},\quad\frac{\rho_i}{L}\ll1,$$

was used to remove the equilibrium quantities out of the dr integrals. Eq. (4.5) is the low frequency perpendicular force balance equation. Specifically, Eq. (4.5) can be recast into

$$\frac{\delta B_\parallel B_0}{4\pi}+2\pi\Omega_i^2\int d\mu dv_\parallel\Big(B_0\Big\langle\int_0^\rho\delta Frdr\Big\rangle+\frac{F_0}{\rho_i^2}\Big\langle\int_0^\rho\Big\langle\int_0^\rho\delta B_\parallel r'dr'\Big\rangle rdr\Big\rangle\Big)=0.\tag{4.6}$$

The first term is the perturbed magnetic pressure, which is balanced by the perturbed particle pressure. The perturbed particle pressure consists of a perturbed gyrocenter

pressure (the second term) and another component (the third term) arising from the coordinate transformation between gyrocenter and particle coordinates. The origin of this additional component is the perpendicular current from the imbalance between ion and electron $\mathbf{E}_\perp \times \mathbf{B}$ drifts due to the ion finite Larmor radius effects [11, 19]. Here $\mathbf{E}_\perp = -c^{-1}\partial \mathbf{A}_\perp / \partial t$ is the inductive electric field from the first time derivative of the perpendicular vector potential $\mathbf{A}_\perp$. The second time derivative of $\mathbf{A}_\perp$, which gives rise to the fast magnetoacoustic wave [24], has been dropped as a result of the frequency ordering.

As discussed in the next section, the integral over δF may be numerically evaluated using the method of Section 3, but a different technique needs to be used for the μ-integral in the second term on the left-hand side of Eq. (4.5). Again, the numerical method may be verified against an analytic result by representing the transformation to particle phase space by $e^{-i\mathbf{r}\cdot\mathbf{k}_\perp}$, which results in

$$\begin{aligned}
&\frac{8\pi^2\Omega_i^2}{\rho_i^2 B_0}\int d\mu dv_\parallel F_0 \Big\langle \int_0^\rho \Big\langle \int_0^\rho \delta B_\parallel r' dr' \Big\rangle r dr \Big\rangle \\
=&\frac{\beta\delta B_\parallel}{2k_\perp^4\rho_i^4}\int_0^\infty e^{-x}\Big\langle \int_0^{k_\perp\rho_i\sqrt{2x}} \Big\langle \int_0^{k_\perp\rho_i\sqrt{2x}} e^{iu'\cos\xi} u' du' \Big\rangle e^{-iu\cos\xi} u du \Big\rangle dx \\
=&\beta\delta B_\parallel \frac{1}{k_\perp^2\rho_i^2}\int_0^\infty e^{-x} x J_1^2\big(k_\perp\rho_i\sqrt{2x}\big) dx \qquad (4.7)\\
=&\beta\delta B_\parallel \big[I_0(k_\perp^2\rho_i^2) - I_1(k_\perp^2\rho_i^2)\big] e^{-k_\perp^2\rho_i^2}, \qquad (4.8)
\end{aligned}$$

where $u = rk_\perp$, $x = \mu B_0/T_i$, $\beta = 8\pi n_0 T_i/B_0^2$, I_n is the n^{th} order Modified Bessel function of the first kind, and the $v_\parallel$ integration was performed explicitly. Comparing (4.7) to (4.8), the objective is to find the numerical approximation of the left-hand side of

$$\frac{1}{k_\perp^2\rho_i^2}\int_0^\infty e^{-x} x J_1^2\big(k_\perp\rho_i\sqrt{2x}\big) dx = \big[I_0(k_\perp^2\rho_i^2) - I_1(k_\perp^2\rho_i^2)\big] e^{-k_\perp^2\rho_i^2}, \qquad (4.9)$$

to reproduce the result on the right-hand side as closely as possible.

4.2 Numerical implementation

Numerical implementation involves discretization of the integrals of Eq. (4.5) over the surface enclosed by the gyro-orbit. The term involving δF may be approximated using the same method as outlined in Section 3. However, the second term on the left-hand side contains an integral over the magnetic moment whose integrand depends on μ through the equilibrium distribution function F_0, and through the upper limits of the r-integrals. A method similar to the one devised in [21] may be used to approximate this integral. The method enables expressing the perpendicular Ampere's law in a matrix form, which may then be solved for $\delta B_\parallel$ using standard numerical techniques.

The approximation may be obtained by discretizing the integrand on the left-hand side of Eq. (4.9) as,

$$\frac{1}{k_\perp^2\rho_i^2}\int_0^\infty e^{-x}xJ_1^2\left(k_\perp\rho_i\sqrt{2x}\right)dx\approx\frac{1}{k_\perp^2\rho_i^2}\int_0^\infty\sum_{s=1}^{S}c_s\delta(x-x_s)xJ_1^2\left(k_\perp\rho_i\sqrt{2x}\right)dx$$
$$=\frac{1}{k_\perp^2\rho_i^2}\sum_{s=1}^{S}c_sx_sJ_1^2\left(k_\perp\rho_i\sqrt{2x_s}\right). \tag{4.10}$$

The deviation of the numerical approximation from the exact analytic result may be represented by,

$$\int_0^{k_\perp\rho_i|_{\max}}\left(\left[I_0(k_\perp^2\rho_i^2)-I_1(k_\perp^2\rho_i^2)\right]e^{-k_\perp^2\rho_i^2}-\frac{1}{k_\perp^2\rho_i^2}\sum_{s=1}^{S}x_sJ_1^2\left(k_\perp\rho_i\sqrt{2x_s}\right)c_s\right)d(k_\perp\rho_i). \tag{4.11}$$

Since it is desirable that the approximation is best for $k_\perp\rho_i\to0$, the optimal values of c_s and x_s may be determined by expanding both sides of Eq. (4.9) in the limit $k_\perp\rho_i\to0$,

$$\left[I_0(k_\perp^2\rho_i^2)-I_1(k_\perp^2\rho_i^2)\right]e^{-k_\perp^2\rho_i^2}\approx1-\frac{3}{2}k_\perp^2\rho_i^2+\mathcal{O}(k_\perp^4\rho_i^4), \tag{4.12a}$$

$$\frac{1}{k_\perp^2\rho_i^2}\sum_{s=1}^{S}x_sJ_1^2\left(k_\perp\rho_i\sqrt{2x_s}\right)c_s\approx\sum_{s=1}^{S}\frac{x_s^2c_s}{2}\left(1-\frac{x_s}{2}k_\perp^2\rho_i^2\right)+\mathcal{O}(k_\perp^4\rho_i^4), \tag{4.12b}$$

and matching the lowest order terms. From the two lowest orders, the constraints on c_s and x_s were thus found to be

$$2=\sum_{s=1}^{S}x_s^2c_s, \tag{4.13a}$$

$$6=\sum_{s=1}^{S}x_s^3c_s. \tag{4.13b}$$

The constraints (4.13a) and (4.13b) decrease the number of degrees of freedom by two, yielding

$$c_1=\left(2-\sum_{s=2}^{S}x_s^2c_s\right)^3\left(6-\sum_{s=2}^{S}x_s^3c_s\right)^{-1}, \tag{4.14a}$$

$$x_1=\left(6-\sum_{s=2}^{S}x_s^3c_s\right)\left(2-\sum_{s=2}^{S}x_s^2c_s\right)^{-1}. \tag{4.14b}$$

The optimum values of $\{c_s,x_s\}$, are those that minimize (4.11), given the constraints (4.14a) and (4.14b), for some desired S.

To decrease the computational cost, the number of grid points, S, should be as low as possible. For $S=1$, the Eqs. (4.14a) and (4.14b) give $c_1=2/9$ and $x_1=3$. The approximation

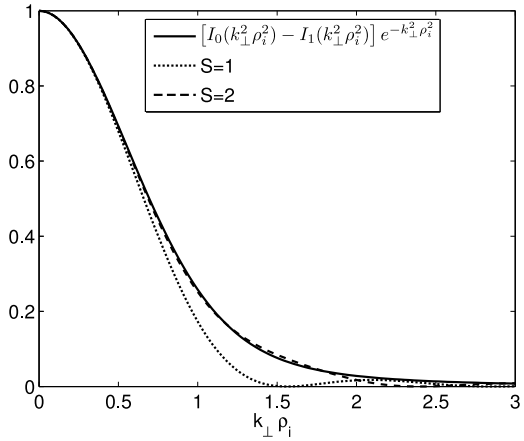

Figure 5: Comparison of the approximation of Eq. (4.8) (solid line) by Eq. (4.10), for $S=1$ and $S=2$ (dotted line and dashed line, respectively). S is the upper limit of the sum in Eq. (4.10), and corresponds to the number of grid points in the $x=\mu B_0/T_i$ variable.

is significantly improved for $S=2$. These results are shown in Fig. 5, according to which, for $k_\perp\rho_i \lesssim 2$, the integral over magnetic moment, appearing in the perpendicular force balance equation (4.5), is well approximated by two points at $x_s=\{4.268,1.278\}$, with the weight of $c_s=\{0.0632,0.518\}$. The surface integrals appearing in (4.5) may be performed using the method outlined in Section 3, with the corresponding values of $\rho_s=\rho_i\sqrt{2x_s}$.

5 Conclusions

The finite Larmor radius effects in gyrokinetic simulations of low frequency compressional modes, may be included by expressing the gyrokinetic model entirely in terms of $\delta B_\parallel$. This introduces a gyro-surface average operation into the equations of motion. For long wavelength perturbations, it has been demonstrated that it is sufficient to approximate the surface integral using the 4-point gyro-orbit averaging technique at an effective gyroradius. In addition, the perpendicular Ampere's law may be expressed as the low frequency perpendicular force balance equation, and the resulting magnetic moment integral may be approximated by carefully choosing samples in the μ-coordinate, and their corresponding weights. The method may be used in gyrokinetic simulations of low frequency compressional modes in space or laboratory plasmas, and has been used to study the drift compressional mode [23].

Acknowledgments

This work was supported by National Science Foundation and U.S. Department of Energy grants. We acknowledge useful discussions with Alain Brizard, Liu Chen, T. S. Hahm, Roger McWilliams and Hong Qin.

References

[1] T. M. J. Antonsen and B. Lane, Kinetic equations for low frequency instabilities in inhomogeneous plasmas, Phys. Fluids., 23 (1980), 1205–1214.
[2] E. V. Belova, R. E. Denton and A. A. Chan, Hybrid simulations of the effects of energetic particles on low-frequency mhd waves, J. Comput. Phys., 136 (1997), 324–336.
[3] A. Brizard, Nonlinear gyrokinetic maxwell-vlasov equations using magnetic coordinates, J. Plasma. Phys., 41 (1989), 541–559.
[4] A. Brizard, Nonlinear gyrofluid description of turbulent magnetized plasmas, Phys. Fluids. B., 4 (1992), 1213–1228.
[5] A. J. Brizard and T. S. Hahm, Foundations of nonlinear gyrokinetic theory, Rev. Mod. Phys., 79 (2007), 421–468.
[6] J. R. Cary and A. J. Brizard, Hamiltonian theory of guiding-center motion, Rev. Mod. Phys., 81 (2009), 693–738.
[7] P. J. Catto, Linearized gyro-kinetics, Plasma. Phys., 20 (1978), 719–722.
[8] L. Chen and A. Hasegawa, Kinetic theory of geomagnetic pulsations I-internal excitations by energetic particles, J. Geophys. Res., 96 (1991), 1503–1512.
[9] C. Crabtree and L. Chen, Finite gyroradius theory of drift compressional modes, Geophys. Res. Lett., 31 (2004), L17804.
[10] E. A. Frieman and L. Chen, Nonlinear gyrokinetic equations for low-frequency electromagnetic waves in general plasma equilibria, Phys. Fluids., 25 (1982), 502–508.
[11] T. S. Hahm, L. Wang and J. Madsen, Fully electromagnetic nonlinear gyrokinetic equations for tokamak edge turbulence, Phys. Plasmas., 16 (2009), 022305.
[12] A. Hasegawa, Drift mirror instability in the magnetosphere, Phys. Fluids., 12 (1969), 2642–2650.
[13] A. Hasegawa, Plasma instabilities in the magnetosphere, Rev. Geophys., 9 (1971), 703–772.
[14] I. Holod, W. L. Zhang, Y. Xiao and Z. Lin, Electromagnetic formulation of global gyrokinetic particle simulation in toroidal geometry, Phys. Plasmas., 16 (2009), 122307.
[15] N. Joiner, A. Hirose and W. Dorland, Parallel magnetic field perturbations in gyrokinetic simulations, Phys. Plasmas., 17 (2010), 072104.
[16] M. Kotschenreuther, G. Rewoldt and W. M. Tang, Comparison of initial value and eigenvalue codes for kinetic toroidal plasma instabilities, Comput. Phys. Commun., 88 (1995), 128–140.
[17] W. W. Lee, Gyrokinetic particle simulation model, J. Comput. Phys., 72 (1987), 243–269.
[18] W. W. Lee and H. Qin, Alfven waves in gyrokinetic plasmas, Phys. Plasmas., 10 (2003), 3196–3203.
[19] Y. Lin, X. Wang, Z. Lin and L. Chen, A gyrokinetic electron and fully kinetic ion plasma simulation model, Plasma. Phys. Control. Fusion., 47 (2005), 657.
[20] Z. Lin, T. S. Hahm, W. W. Lee, W. M. Tang and R. B. White, Turbulent transport reduction by zonal flows: massively parallel simulations, Science., 281 (1998), 1835–1837.
[21] Z. Lin and W. W. Lee, Method for solving the gyrokinetic poisson equation in general geometry, Phys. Rev. E., 52 (1995), 5646–5652.
[22] S. E. Parker, Y. Chen, W. Wan, B. I. Cohen and W. M. Nevins, Electromagnetic gyrokinetic simulations, Phys. Plasmas., 11 (2004), 2594–2599.
[23] P. Porazik and Z. Lin, Gyrokinetic particle simulation of drift-compressional modes in dipole geometry, sumbitted to Phys. Plasmas., (2011).
[24] H. Qin, W. M. Tang, W. W. Lee and G. Rewoldt, Gyrokinetic perpendicular dynamics, Phys.

Plasmas., 6 (1999), 1575–1588.
[25] H. Qu, Z. Lin and L. Chen, Gyrokinetic theory and simulation of mirror instability, Phys. Plasmas., 14 (2007), 042108.
[26] M. N. Rosenbluth, Magnetic trapped-particle modes, Phys. Rev. Lett., 46 (1981), 1525–1528.
[27] P. H. Rutherford and E. A. Frieman, Drift instabilities in general magnetic field configurations, Phys. Fluids., 11 (1968), 569–585.